Scaled Down Hyperloop Prototype Pod Design: Design Comparison Analysis on the Dynamic and Braking System

Mahek Logantha, Myron Phan, Nathan Bernardo, Leanna Hao, David Villalpando, Kaushal Patel, Sarah Graves, Rahul Sheth, Vikram Bhave, Christine Tran, Bobby Laviguer

HyperXite
University of California, Irvine
August 18,2020

I. ABSTRACT

The Hyperloop pod is a vehicle that is set to revolutionize the technological advancement of transportation systems. Like the bullet train, it is meant to transverse from point A to B at a tremendous speed, making it convenient for people that rely on transportation systems for traveling and commuting. However, the Hyperloop pod is designed to travel through a vacuum tube to negate air friction so that the pod can achieve high accelerations. Ideally, the concept compensates the practical modes of transportation by being relatively inexpensive compared to airfares and fast compared to public transportation methods. The HyperXite team has been building scaled-down prototype pods for the past four years with this Hyperloop vision in mind.

After determining that building a full prototype pod would not be feasible for the team this year given the state of the competition and budgetary constraints, the team decided to move forward with a scaled down version of the pod with design concepts that we wanted to test.

We set a loose requirement of a 3 foot long pod that would still be able to move along the I-beam track with the given dimensions from the 2019 SpaceX Hyperloop competition. The pod stands at 62.36 inches in length, 30.137 inches in width, 17.452 inches in height, and its current mass is approximately 120lbs.

We moved forward with a dual motor design, friction brakes that are actuated by our pneumatic system, and an aluminum chassis. Figure 1 provides an overview of the mechanical subsystems that make up the Hyperloop pod.

Not having SpaceX Competition design requirements to follow, gave our team the freedom to test different designs for each subsystem. The most drastic design changes have been implemented in the Dynamics and Braking subsystems. Specifically, the following paper provides a design comparison analysis between Pod IV (2019 pod) and Pod V's dynamic and braking system, highlighting the Pod IV's system, performance analysis, cost analysis, and feasibility.
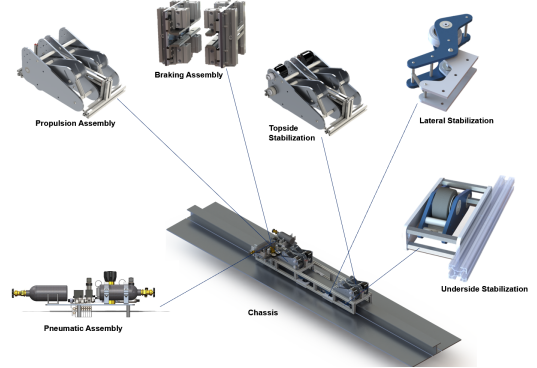

FIG. 1: Mechanical Subsystems of the Pod

II. DYNAMICS

A. Overview of Pod IV Dynamics

Pod IV utilized a single permanent magnet synchronous motor (PMSM) mounted directly to the drive wheel with the drive and driven shafts connected via a gear coupling. The wheel and motor fasten to the center of the pivot arms with one side of the arms attached to the chassis and the other end isolated from the chassis through the use of motorcycle grade coilovers. This design takes advantage of the flat torque vs RPM curve provided by the PMSM to accelerate the pod rapidly and smoothly to its top speed. However, the size of the PMSM required a relatively tall suspension armature, inducing large bending moments throughout the propulsion unit during acceleration. Additionally, the PMSM required adjustable frequency drive control which proved overly complex for our application and greatly impeded development of the controls for the pod.

As for the stabilization units, the Pod IV topside stabilization employed coilover suspension, the lateral used tension springs, and the underside lacked any suspension method. The lack of compliance in the underside suspension required the mounts to be far thicker than the others to prevent material failure. These design choices simplified the assemblies under the assumption that the pod would undergo minimal vibration during its run. We verified the structural integrity of the suspension by simu-
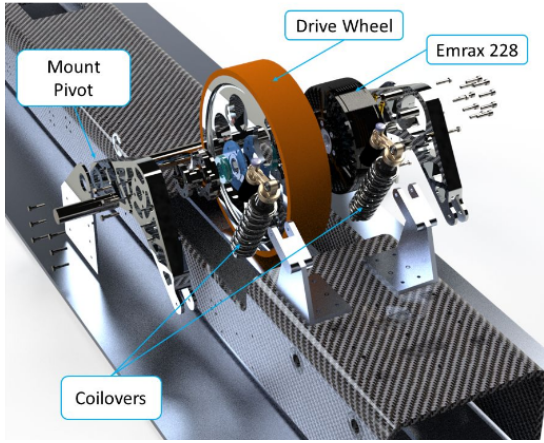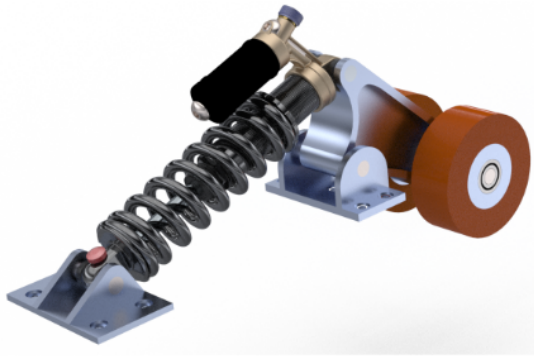
FIG. 2: Propulsion for Pod IV

FIG. 3: Topside Stabilization for Pod IV

lating the stresses throughout each unit when under maximum load, which resulted in a minimum factor of safety of 3.07 for the underside, 3.33 for topside, and 5.01 for lateral.

B. Overview of Pod V Propulsion

The propulsion system for Pod V emphasizes compact and cost effective design employing dual brushless direct
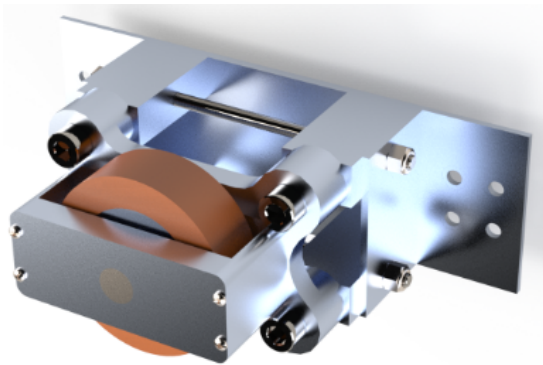

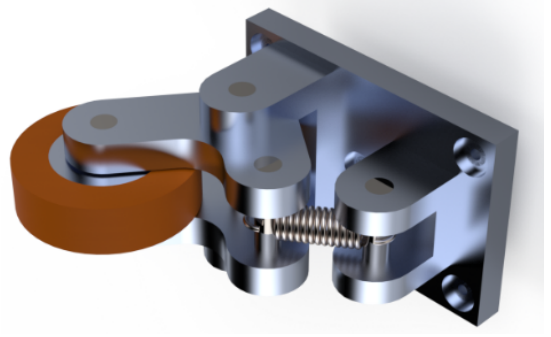FIG. 4: Underside Stabilization for Pod IV
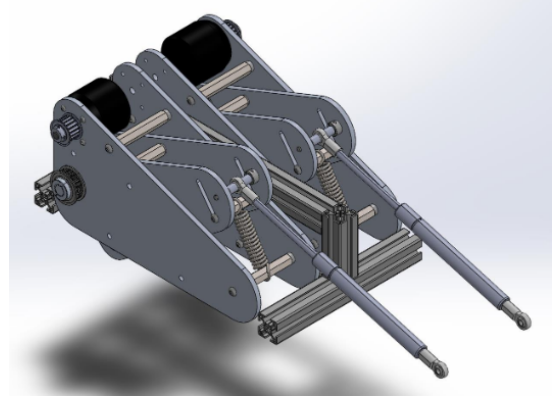

FIG. 5: Lateral Stabilization for Pod IV

FIG. 6: Propulsion for Pod V

current (BLDC) motors and tension spring suspension. The mounting plate is $\frac{3}{8}$ inch steel in the shape of a right triangle oriented with the one leg aligned with and fastened to the chassis, and the other leg aimed towards the top of the pod. The motor mounts at the top of this plate and connects to the drive shaft through two timing belts, one from the motor to the pivot and one from the pivot to the drive shaft. The pivot arm assembly also takes on triangular design and sits between two of the mounting plates. The pivot arm houses the wheel at the 90° vertex and connects to the chassis at the pivot on the near vertex and to the tension spring suspension on the other. This propulsion unit is mirrored to provide adequate torque during the acceleration phase of the pod run, while also reducing the number of bespoke components and lowering manufacturing costs. Aluminum extrusions are used to secure the two propulsion units to one another and allow assembly to occur separately from the chassis, making the design highly modular.

C. Overview of Pod V Stabilization

In total, Pod V utilizes 12 stabilization units to follow the track and isolate the chassis from excitation due to track defects. The propulsion units work together with the top and underside stabilization to clamp the flange of

the I-beam track to maintain traction during the pod's acceleration and deceleration phases and to prevent the pod from colliding with the track during bump events. The remaining 4 stabilization units clamp the web of the I-beam to keep the pod centered on the track and to mitigate the deflection due to any defects in the track. A MATLAB Simulink model of Pod V will be created to select spring and damping constants for the stabilization units and to verify that the stabilization keeps all deflections within the maximum values. Once pod manufacture and testing begins this model will undergo validation by comparing simulated results with pod performance results.
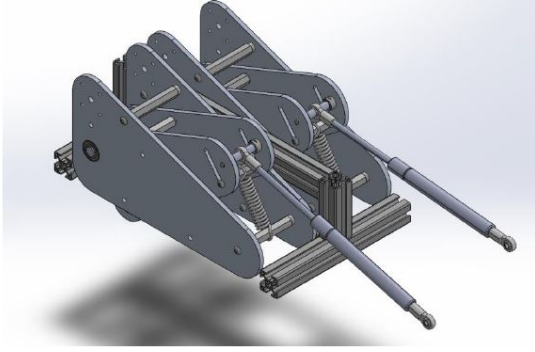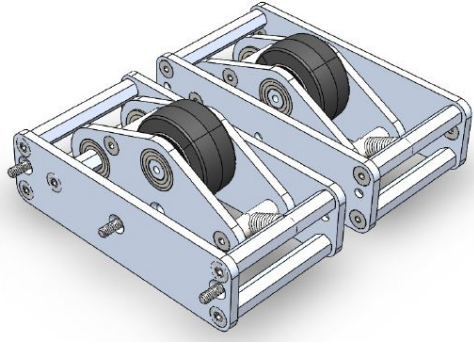

FIG. 7: Topside Stabilization Unit

FIG. 8: Underside Stabilization Unit

D. Performance Analysis

We created a MATLAB script to simulate the Pod V trajectory for a variety of projected masses on a 20 meter long track. The purpose of this simulation was to roughly estimate the top speed of Pod V and the maximum downforce required for traction, thus we neglected all frictional losses. Taking the average performance values, Pod V is projected to accelerate at a maximum of 0.27 G's, reaching a peak velocity of 8.9 m/s immediately before beginning the braking phase. At this acceleration,
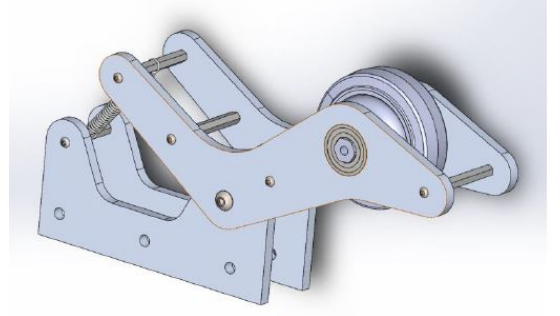

FIG. 9: Lateral Stabilization Unit

the polyurethane wheels we selected have a sufficient coefficient of friction to maintain a no slip condition with the I-beam throughout the run.

E. Feasibility

Dynamic structures for Pod IV cost approximately 17000 USD and aimed for a maximum velocity of 104 m/s. Dynamics for Pod V is estimated to cost 2600 USD and reach a maximum velocity of 8.9 m/s. Pod IV produces approximately 0.006 m/s per USD, while Pod V predicts a ratio of 0.003 m/s per USD, representing a 50% loss in cost efficiency from Pod IV to Pod V. We account for this reduction in efficiency by considering the difference in parameters for the two pods. Pod IV's dynamics budget was 6.5 times that of Pod V, and planned to run on a one mile long track in comparison to the 20 meter long track for Pod V. These discrepancies, coupled with the size constraints imposed by a small-scale pod, reduce the maximum attainable velocity for Pod V and reinforce design choices that sacrifice performance for cost.

Pod V's dynamic systems emphasize compact and modular design to reduce manufacturing costs and allow for rapid iteration and testing. The propulsion and topside stabilization units are standalone and may be removed from the chassis intact, making assembly, tuning, and testing highly flexible. The transition from Pod IV to Pod V came with an 85% reduction in the dynamics budget, necessitating creative design to maximize performance while meeting cost constraints.

III. BRAKING

A. Overview and Critique of Pod IV Braking

Pod IV was equipped with an eddy-current magnetic braking system [Fig 10]; two magnetic Halbach Arrays were oriented on either side of the conductive I-beam to provide a braking force without contact to the track. The permanent magnetic array, when moving in relation
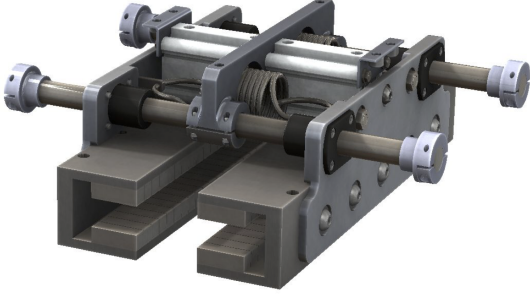
FIG. 10: Braking Mechanism for Pod IV

FIG. 11: Braking Mechanism for Pod V

to the aluminum track, induces eddy currents in the I-beam[1]. These eddy currents generate drag force.

There are distinct benefits to the permanent magnetic braking system, including its ability to operate without need of external power or other electrical components. Pod IV's system was designed to be engaged if not powered, providing a truly redundant design in the event of a power loss to the system. Since eddy current braking is non contact, the system encounters less mechanical stresses and overall wear to the system. A magnetic braking system is said to have a lower maintenance cost and longer service life than typical friction designs [2].

Though a eddy-current magnetic braking system can produce great drag forces under many conditions, the eddy currents also produce a large lift force if the two halbach arrays are not properly balanced. The nature of permanent magnets also stops it's ability to adapt to different braking force perfomance needs, so if the braking force is needed to be lighter for a more gradual stop or increased the system cannot change its parameters[2]. The braking force is dependent on the speed of the pod rather than the input of any user. So, this leads to a very consistent system, but inflexible in terms of design.

A magnetic braking design is not ideal for our current design due to both its high weight and the tight tolerances that it forces on the pod's stabilization, as well. Due to the narrow gap between the track and the permanent magnets, the allowable vertical oscillation of the pod was greatly limited. This led to a very rigid stabilization design and excess stress on the Pod's structure.

In the scope of a fully realized Hyperloop design, the team acknowledges that a magnetic braking system may be the safest and most reliable option. However, within the constraints of a scaled down scope in terms of both pod size and budgetary constraints, a pneumatic friction braking system is ideal for our current design.

B. Design Overview

Pod V implements a pneumatically actuated friction braking system that creates a friction drag force by clamping onto the flanges of the I-beam. The design consists of two sets of fo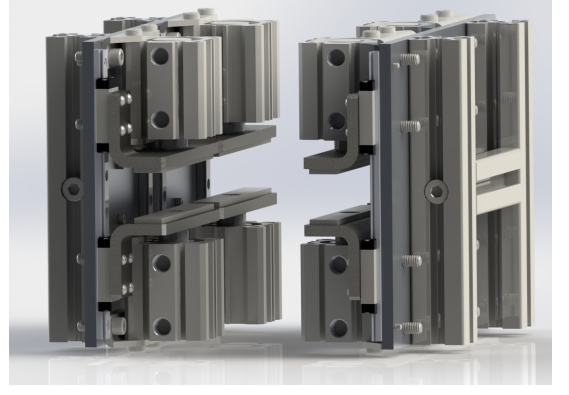ur actuators oriented on opposite sides of the I-beam. These are then mounted onto aluminum plates and connected to the aluminum extrusions of the chassis. The braking system can be further broken down into 4 linear rail sub-assemblies consisting of 2 actuators on opposite sides of the I-beam and a brake pad mounted to 2 linear rails [Fig 12]. These linear rails provide rigidity to the system creating a force path through the linear rails to the rest of the system rather than allowing the force to concentrate on the actuator rod. The
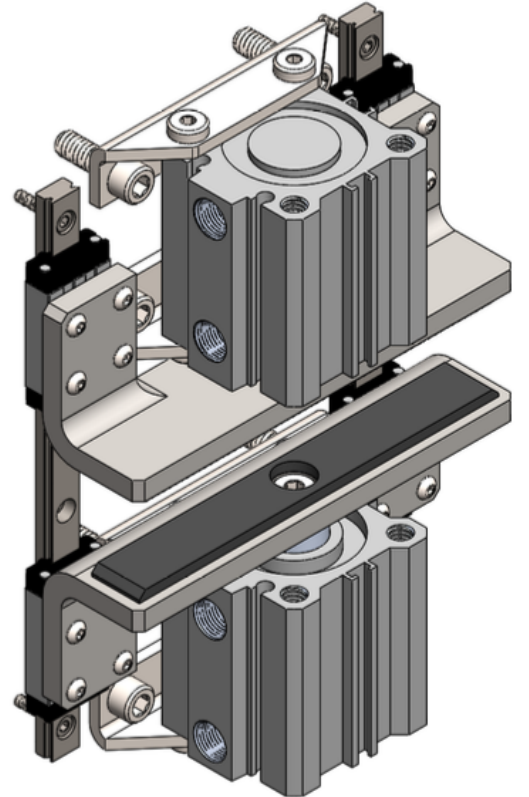

FIG. 12: Linear Rail sub-assembly

dual linear rail design is ideal for mitigating the bending moment caused by the braking force. A single linear rail design would only be able to create a horizontal reaction

force in the x-direction to resist the braking force, creating a clockwise bending moment that the braking structure must resist. However, the dual linear rail design introduces a vertical component to the linear rail reaction forces, the blue forces in the z-direction in Fig. 13. The z-direction reaction forces create a counter-clockwise moment around the z-axis to resist the clockwise moment that the braking force and horizontal linear rail reaction forces create.
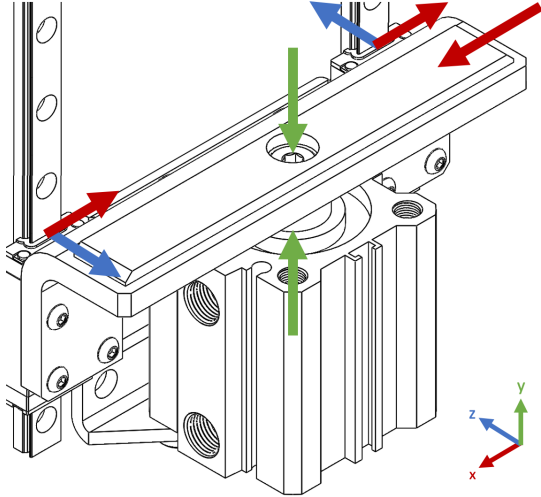

FIG. 13: Dual Linear Rail Free Body Diagram, action-reaction pairs are notated by the same color

To ensure that the braking system does not damage the track, the brake pad material must have a lower hardness than 95 Brinell or 276 MPa, the hardness values of Aluminum 6061-T6. Only brake lining material was considered, as it is designed to wear away when exposed to high friction forces rather than adhere to the contact material and damage the track. The remaining material candidates were then compared based on their friction coefficient, as a higher friction coefficient results in a greater breaking force. The material chosen, Bremskerl 5505, has a hardness value of 39.9 MPa and a friction coefficient of 0.47. The material has a maximum operating temperature of 480 degrees Farenheit for continuous braking and 750 degrees Farenheit for intermittent braking, which, due to the short length of the test track and the calculated engagement time being approximately 0.4 seconds, it is very unlikely the material will reach these temperatures in a single run and brake fade is not expected to occur.

Half of the actuators sit within the bounds of the I-beam, so improper orientation of the actuator ports would result in pneumatic connectors and piping possibly coming into contact with the web of the I-beam. For ideal placement of the air ports and to prevent undue costs from manufacturing specialized parts for mounting, an actuator with flexible mounting was required. Actuator bore size was decided based on the the original acceleration goal of 2 G's (2 magnitudes of gravity),

a Factor of Safety of 2, the assumption of a 50 kg pod, and a working psi of 100. Calculations based on these values required a minimum bore diameter of about 1.18 in., which was rounded up to 1.25 in. to match common actuator bore sizes.

The linear rails were chosen based on the maximum yaw across the braking system caused by the braking force, as this is expected to be the greatest moment the system experiences. Based on our preliminary calculations mentioned when selecting an actuator, a single linear rail assembly experiences 490 N of braking force and about 12 Nm of bending moment. Making the assumption that the linear rails split the bending moment somewhat evenly, each linear rail can be expected to withstand about 6 Nm of bending moment. Though this assumption isn't true in reality, the simplification was made in order to make linear rail selection simpler. The current linear rails are rated to withstand 13 Nm of bending moment. Simulations were run to validate these choices.

C. Performance Analysis

The maximum allowable moment around the y-axis of the linear rails being about 6.15 Nm, this limits the actuator operating pressure to 76.7 psi. Braking calculations were completed based on the current pod statistics: pod mass of 120 lb and a peak velocity of 25 mph.

- Stopping Rate: 2.95 G's

- Engagement Time 0.31 s

- Stopping Distance: 1.38 m

Simulations were ran on the aluminum 6061 mounting plate connecting the linear rail sub assemblies to the aluminum extrusions of the chassis.
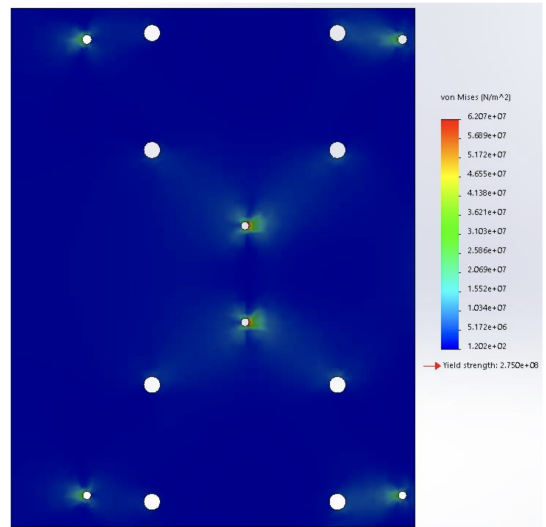

FIG. 14: Von Mises Stresses on the Braking Carrier Plate

The applied external loads in this simulation are a 530N bearing load applied on the linear rail set holes, an overestimation of the shear force experienced by a linear rail subsystem, and a 1060N bearing load on the extrusion holes, representing the transfer of force from the 2 linear rail sub assemblies to the chassis. The maximum bearing loads follow a factor of safety of 2, and no significant damage occurred. The actuator foot bracket holes, see the largest diameter holes found in 4 sets of 2, are simulated as fixtures.
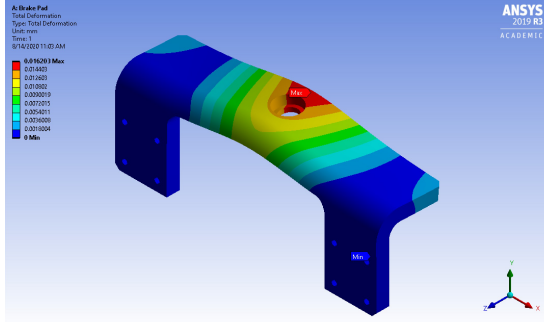

FIG. 15: Total Deformation on Brake Pad Mount

Simulations were performed in Ansys Mechanical on a Low Carbon 1018 Steel brake pad mount to determine the total deformation, stress and bending moment reactions that would result for the given loading conditions. Low Carbon 1018 Steel has a Young' Modulus = 2.1E5 MPa and a Poisson's Ratio = 0.290.

When the system is activated, an actuating force pushes the brake pad mount with braking lining into the flange of the I-beam causing both a braking shear force and a counteractive normal force. To simulate the braking force, a shear force of 191.25N was applied to the top plate of the brake pad mount. The actuating force is simulated as a concentrated force acting near the hole of the threaded fastener, and a distributed normal force of 425N was applied to the top plate of the brake pad mount. The linear rail holes on the wide flanges were treated as fixed supports in this simulation.

The actuator shaft and brake pad mount are fastened to one another via a 5/16"-24 hex screw, so a counterbore was added in the brake plate to ensure that the screw will not contact the track. The brake plate thickness underneath the hex screw is approximately 2mm and the clearance between the hex screw and the top of the brake plate is about 0.1 mm. A big concern was that the counterbore would weaken the overall brake pad mount, however the maximum stress applied is 51.655 MPa which yields a minimum factor of safety (FS) = 6.4.

The reaction moment in the z-axis is of primary importance and has a value of Mz = 5.295 Nm for the given loading conditions, as it is the largest moment that the structure must resist. This still meets the minimum factor of safety requirement of 2, since the maximum allowable moment in that direction is 12.1 Nm. Given the loading parameters and fixed supports, the following results were

obtained:

- Max Deformation (mm): 0.016203

- Stress (MPa):
    - Max = 51.655.
    - Min = 5.516E-4.

- Moment Reaction (N*mm):
    - X = 0.130
    - Y = 3.309
    - Z = 5.259
    - Total = 6.216

In order to validate the simulation results, moment resultant calculations were completed based on the free body diagrams in Fig. 16 and 17. The Resultant Z moment was calculated to be 5.43 Nm clockwise and the Resultant Y moment was 3.88 Nm counterclockwise. Which are both within the same magnitude as the simulated results. The percent error between the different results is 3.25% for the Z moment and 17.2% for the Y moment respectively. The slightly higher percent error in the Y moment can be attributed to the moments created by internal stresses that the free body diagram in Fig. 17 does not account for, as the system is expected to produce a resistant moment but is unable to produce an external reaction force. There are plans to test the
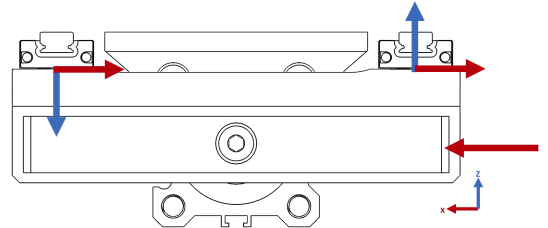

FIG. 16: Top Dual Linear Rail Free Body Diagram, action-reaction pairs are notated by the same color

Braking system on a braking test rig consisting of aluminum disc with the same thickness at the I-beam flange propelled by a brushless DC motor. With this setup, the efficiency of the brake pads can be studied for factors such as Peak braking force, continuous power dissipation, fade, smoothness, etc. Results from the test rig will be compared to the results obtained from simulations to validate and improve our design further.

D. Feasibility

The permanent magnet arrays used in Pod IV's braking design cost 9500 USD; the entire design, including manufacturing costs and materials, was approximately 12000 USD. This braking system could reach a maximum drag force of around 2500 N. In comparison, Pod
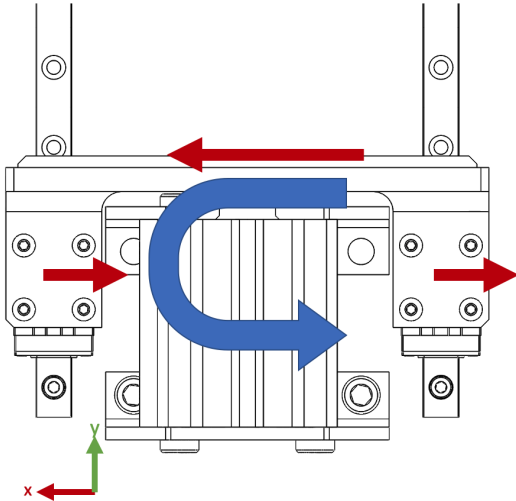
FIG. 17: Front Dual Linear Rail Free Body Diagram, action-reaction pairs are notated by the same color

FIG. 18: Pneumatic System (Top)

FIG. 19: Pneumatic System (Side)

V's pneumatic friction braking system is approximately 1000 USD and has a maximum braking force of around 2000 N. They both provide about 2 N of drag force per USD, with the current design being 1/12th the cost of the magnetic braking design.

Pod IV's braking system was designed to be easy to test and iterate upon. A friction braking system can be easily tuned by varying operating pressure and the system itself was designed to be easy to disassemble and reassemble if needed, and can even be taken entirely out of the pod fully in a fully assembled state by unfastening the aluminum extrusions at the back from the main chassis for easy testing. The variability of a pneumatic friction design and lower cost of the components make an ideal design for a smaller pod that will undergo rigorous testing and alterations.

E. Piping and Cooling

The purpose of the Piping and Cooling System is to provide the necessary air pressure to the braking system in order to engage and disengage the brakes. As we design the pneumatics system, we are taking two modes into consideration; one mode where power is being supplied to the pod and one mode with a loss of power to the pod. In the event of a power-loss, the pneumatic system provides a redundancy that automatically engages the friction brakes. Accordingly, the entire system can be broken down into three main components: pressure reduction, pneumatic redundancy, and actuator connection.
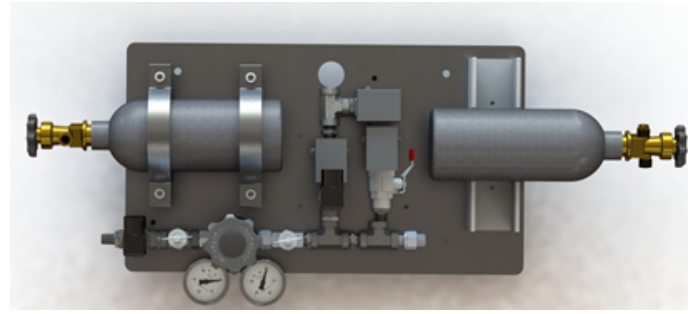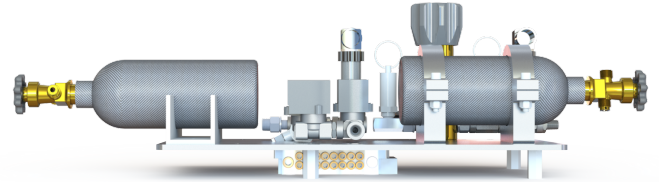
1. Old Pneumatic System vs. New Pneumatic System

With the braking system's decision to switch from magnetic braking to friction braking, the pneumatic system has become increasingly vital to ensuring that the pod comes to a safe stop. With the magnetic braking system, the primary function of pneumatics was to provide the necessary air pressure to disengage the brakes. Since the magnetic braking system also implemented its own redundancy, there was no need for a pneumatic one. With the friction braking system, pneumatics must provide the proper air pressure to both engage and disengage the brakes. Because of this configuration, pneumatics is an integral part of the braking system. Additionally, without a redundancy implemented in the braking mechanism, pneumatics is designing a fail safe within the system to ensure that the brakes are engaged in the event of a pod shut-off. One important aspect of the friction braking fail safe is that it relies on the assumption that there is enough pressure in the compressed air tank to engage the brakes whereas the magnetic braking redundancy does not have this limitation. However, based on preliminary calculations and analysis, we have concluded that both fail safe mechanisms would perform their function to an equal standard and factor of safety.

2. Pressure Reduction

The Pressure Reduction system is the first stage in the pneumatic system to supply pressurized air to the brakes. The system reduces pressure coming from the compressed air tank to the necessary system pressure.
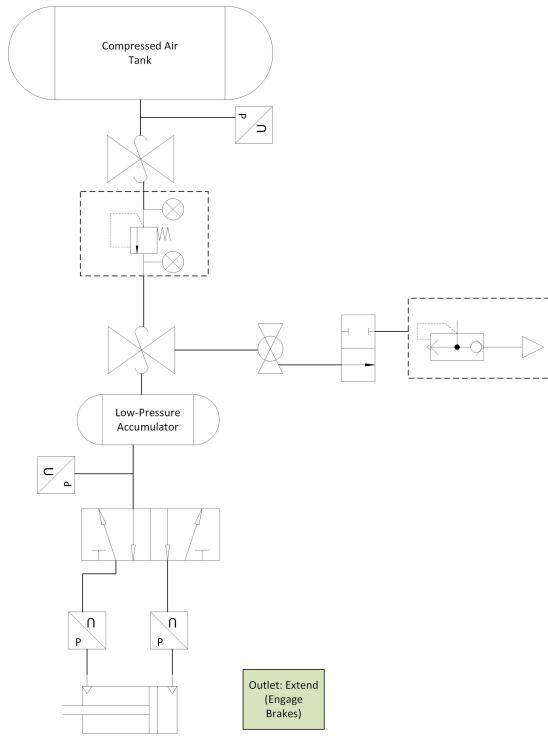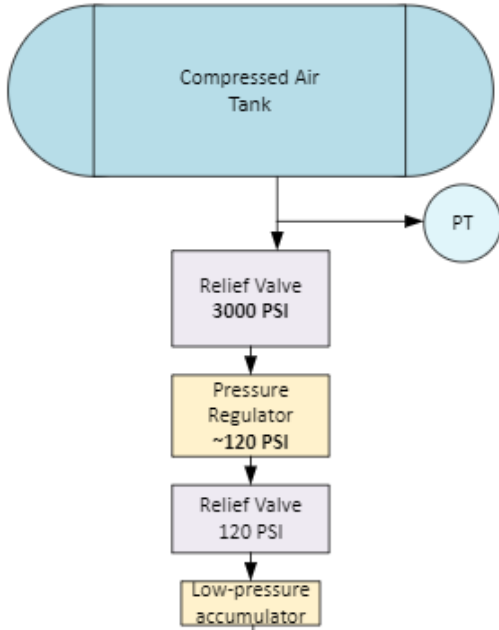
FIG. 20: Official Pneumatics Schematic (Pod Off)

FIG. 21: Pressure Reduction Schematic of Pod V

In Pod IV from 2019, the system was comprised of a compressed air tank with a pressure transducer at the outlet to read and ensure tank pressure was at 2000 psi by controlling the relief valve. Upon exiting the relief valve, the air went through a pressure regulator that decreases pressure to about 120 psi before entering another

relief valve for redundant purposes. In Pod V, the only addition is a low pressure accumulator at the end of system to improve efficiency.

The compressed air tank at the start of the pneumatic system in Pod V holds the pressurized air that will feed the system. The expected pressure of the tank is 2000 psi with a maximum allowable work pressure of 3000 psi. To ensure the pressurized air leaving the tank is 2000 psi, a pressure transducer is at the immediate outlet of the tank. This reading is used to make adjustments to the system to hold the pressure at 2000 psi. If the pressure transducer reads over 2000 psi, the following relief valve with a maximum allowable work pressure of 3000 psi will open to decrease pressure of the line. On the other hand, if the pressure is read to be lower than 2000 psi, the pressure in the tank will be increased manually.

The air then feeds into a pressure regulator with a maximum allowable work pressure of 3000 psi. This regulator takes the 2000 psi from the air tank then decreases it down to 108 psi, the ideal pressure to feed into the braking system. Following the regulator is a relief valve to further ensure the pressure entering the accumulator is 108 psi.

Lastly, the system ends with a low pressure accumulator. This was the only change to the pressure reduction section in Pod IV's design to improve it for Pod V. The accumulator was added to store the 108 psi air at the end of the system. This increases efficiency and speed of the system. By storing air, the actuator connection system can be immediately fed with pressurized air to engage or disengage the brakes rather than take any extra time to wait for the pressure reduction system to produce the low pressure air.

To ensure the system is defined safely, the pressure vessels will have nameplate ratings identifying the maximum allowable work pressures listed above. The system is also dual fault tolerant in its prevention of potential failures in the system. Upon construction of the pod, the system will be both proof tested and leak tested.

3. Actuator Connection

From the Pressure Reduction stage of the Piping and Cooling System, the Actuator Connection stage dispenses the necessary air pressure to the double acting actuators via the base station in order to engage or disengage the brakes.

With the braking system's choice of utilizing eight double acting actuators, multiple solenoid valves are necessary in order to supply the proper air pressure to the brakes. However, with the use of a base station, the pneumatic system can implement multiple solenoid valves without having multiple air inlets from the accumulator tank, thus reducing the complexity and mass on the pod. Our base station is a 5/2 solenoid valve with one inlet, eight outlets, and two exhaust ports that will send air to correct side of each actuator. Once the air is sent from

the accumulator tank, checked by a pressure transducer for the correct air pressure, and sent to the base station, the base station will send air from eight of its sixteen total valves to either engage or disengage the brakes.

A feature of double acting actuators is that air is required to both extend and retract the piston. As such, the base station must provide air to both sides of each actuator which requires two air inlets per actuator. In order to engage the brakes, the air in the disengage outlet must be exhausted and vice versa. This is the basis of our choice for a 5/2 solenoid valve because having a separate exhaust port for engaging and disengaging brakes is required. The solenoid valve is normally open, meaning that when the pod is off, air is supplied to the outlets that engage the brakes. When power is sent to the base station, the valve direction switches and the air that engages the brakes is exhausted while the outlets that disengage the brakes are pressurized. [3]

To ensure the safety of the braking system, namely the double acting actuators, multiple pressure transducers are placed along the Actuator Connection stage. Two pressure transducers are placed after two of the outlets on the base station and before the actuator inlets. This ensures that the correct pressure is being sent to each actuator and that over-pressurization in the outlets does not occur, as this would result in irreparable damage to the actuators and a braking system failure.
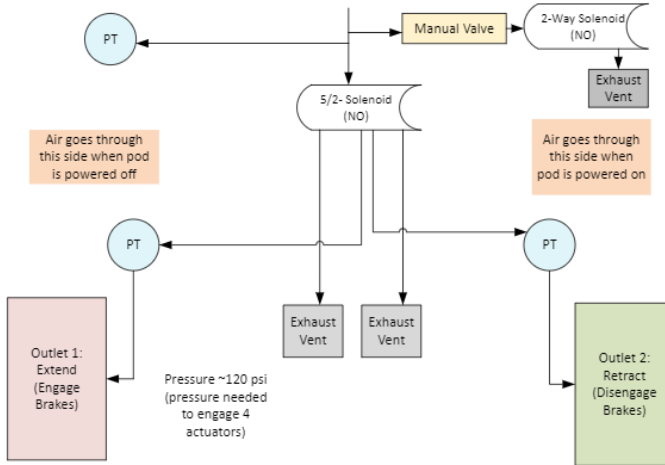

FIG. 22: Actuator Connection and Redundancy Schematic of Pod V

4. Pneumatic Redundancy

When designing the pneumatics system, we are accounting for two modes, one where the pod is supplied with power and one where there is a power loss. The pneumatic redundancy is implemented into the system

to ensure that the brakes are engaged in the event of a power loss to the pod. This is an important safety mechanism for the pod to ensure that if power is lost, the pod does not simply continue at its current velocity.
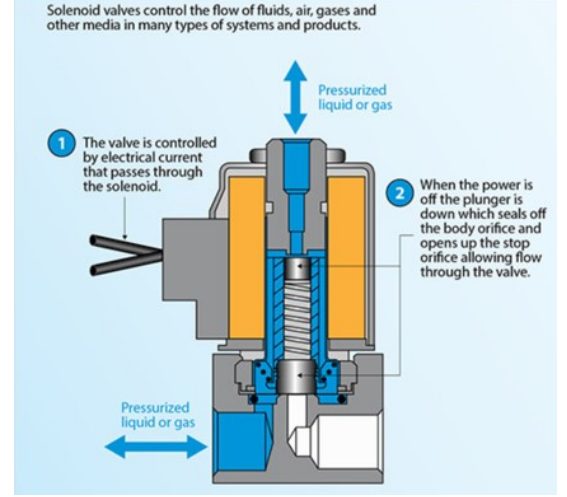

FIG. 23: Normally Closed Solenoid

The fail safe mechanism is implemented as a default position in the pneumatic system. With the choice of a normally open solenoid valve, air is supplied to the outlets that engage the brakes. In the event of a power loss, the base station would revert to an open configuration, allowing pressurization in the outlets that engage the brakes and depressurization in the outlets that disengage the brakes. [4]

IV. CONCLUSION

In this paper, we proposed a more cost effective Hyperloop for prototyping the pod concept with a different dynamic and braking system design. Dynamic systems made the change towards more compact and modular designs for rapid iteration and testing. Not just that, but Pod V propulsion is more cost effective at 0.01 m/s per USD versus 0.006 m/s per USD for Pod IV. From Pod IV to Pod V the braking mechanism changed from magnetic eddy current braking to pneumatic friction braking, a system more suited to the iterative design goals of Pod V. The braking system is just as effective at a fraction of the price as both mechanisms provide about 2 N of braking force per USD, with the current braking system being about 1/12th the price of the permanent magnetic braking system.

V. ACKNOWLEDGEMENTS

———————————————————————

[1] S. J. S. C. Jou, M., Journal of Magnetism and Magnetic Materials **302**, 234 (2006).

[2] T. Y. L. G. L. J. M. I. Chen, Q., Progress In Electromagnetics Research M **61**, 61 (2017).

[3] Tameson, "5/2 4/2-way pneumatic valve - how they work," https://tameson.com/ 52-way-and-42-way-pneumatic-valve.html.

[4] C. Manufacturing, "The difference between normally closed valves and normally open valves," https://www.cpvmfg.com/news/ difference-between-normally-closed-valves-and-normally-open